Materials Science-Poland, 40(4), 2022, pp. 64-77
http://www.materialsscience.pwr.wroc.pl/
DOI: 10.2478/msp-2022-0044

The ability of different types of sand to preserve the integrity of calcium sulfoaluminate cement cement mortar during exposure to elevated temperatures

Jean Jacques Kouadjo Tchekwagep[1,*], Wang Zengyao[1], Yang Fengzhen[1], Zhao Piqi[1], Shifeng Huang[1], Shoude Wang[1], Xin Cheng Cheng[1]

[1]School of Materials Science and Engineering, University of Jinan, Jinan, Shandong 250022, China

Due to the depletion of natural sand resources, it is urgent to develop synthetic sand that will replace the natural one in the production of concrete. In this study, we carried out descriptive inspection of mortar working performance, mechanical properties and internal cracking under three different application schemes of fine aggregate, including natural, artificial, and basalt sand. Tests showed that the mortar with river sand had more internal cracking and lowest strength as the temperature rises. The artificial and basalt sand had better resistance and less internal cracking than river sand at high temperature. The compressive strength of basalt sand mortar (BSM) was slightly higher than that of artificial sand mortar (ASM), while the compressive strength value of river sand mortar (RSM) was the lowest at room temperature. However, when heated to 100°C, the RSM had 48% loss of strength, followed by the BSM at 45.4% and ASM at 11.6%. Above 100°C, none of the mortar samples meet the requirement of the calcium sulfoaluminate cement 42.5. The average atomic ratios (Ca/Si, Ca/Al, and Ca/Si) for the ASM and BSM increased with the rise in temperature. XRD showed that above 100°C, the diffraction peaks of Ettringite (AFt) disappeared, the number of $CaSO_4$ diffraction peaks decreased significantly, the intensity decreased, and a diffraction peak of $CaCO_3$ appeared.

Keywords: *fine aggregate, CSA cement, blend, mechanical performance, heating*

1. Introduction

Due to the world's steadily growing population [1] and an unbroken trend toward urbanization, nearly 40 billion tons of sand are mined each year to meet the growing global demand for building materials [2]. Although this figure is already impressive, the global demand for sand could increase by 45% by 2060 and put this natural resource at risk [3, 4]. As desert sand is unsuitable as a building material [5], it has to be mined or dredged from rivers, deltas, and marine and coastal ecosystems, causing environmental damage [6]. At present, the Chinese government's Department of Natural Resources is paying increasing attention to water and soil protection around rivers, and the exploitation and use of natural river sand are subject to many restrictions [7, 8]. Artificial sand, creating by crushing stone aggregate, is gradually replacing natural river sand in the production of concrete [9, 10]. However, use of artificial sand as concrete fine aggregate has led to problems such as reduced workability, high admixture demand, and increased surface cracking [11, 12], which in turn, has led to extensive research on the performance of this sand [13, 14]. Due to the influence of the grain morphology of artificial sand and the production process [15], the mix proportions of artificial sand concrete are different from the proportions of ordinary Portland concrete (OPC) [16]. The concrete mix proportion needs to solve the above-mentioned problems of poor workability and durability.

In the tropical marine environment [17], concrete structures frequently experience large temperature differences under the alternating effects of sunshine and rainfall [18]. Reports [19, 20] have shown that the surface temperature can be 30 to 50°C higher than the ambient temperature for CSA concrete under direct sunshine, rising as

* E-mail: dadydano@yahoo.fr

high as 90°C under extreme conditions [21]. Rainfall causes the temperature of the concrete structure to drop rapidly [22]. Both high temperature and rapid changes in temperature affect the durability of CSA structures [23]. Recent studies of CSA cement and concrete have shown that heat has a negative impact on CSA structures [24, 25]. As the exposure temperature rises, several deformations have been recorded, characterized by a decrease in strength [26] when the deformation increases as the target temperature rises [27].

Studies of ordinary concrete and reinforced concrete show the extent of temperature effects on durability. The transient thermal deformation of high-performance OPC concrete under various temperatures and load coupling also found that transient thermal deformation occurred only in the first temperature cycle [28]. A study of the mechanical performance evolution of ethylene-vinyl acetate copolymer (EVA) modified concrete found that high temperature reduced the compressive and tensile strength of concrete [29], and EVA can relieve damage due to changing temperatures to some extent [30]. It was found in reinforced OPC concrete samples at alternating temperatures that temperature alternation results in defects such as cracks on steel surface oxides, and it reduces reinforcing concrete interface strength, which affects the durability of the structure [31].

This research study's purpose was to explore the influence of different fine aggregate usage schemes on the performance of CSA mortar when exposed to elevated temperatures; river, basalt and artificial sand were used as the fine aggregates to produce mortar. For the three different types of fine aggregates, we carried out an extensive set of tests, including mechanical strength testing and X-ray diffraction (XRD), X-ray fluorescence (XRF), scanning electron microscopy (SEM), X-ray spectroscopy (EDS), and thermogravimetric (TG) observation of the calcium sulphoaluminate mortar (CSAM). This paper discusses the impact of different fine aggregates on the workability, mechanical properties and durability of CSAM after conditioning at different high temperatures. The paper also considers which type of sand remains most acceptable from an engineering perspective when mixed with CSA and exposed to various high temperatures. The concern is to optimize the stability of the production of CSA structures that might be exposed to high temperature for expanding its life span.

2. Raw materials tests

2.1.1. Characteristics of the different sands used

(a) River sand

In this experiment, the natural sands came from the river, from Gongyi Yuanhengjing Water Supply Factory in China. This sand is characterized by hardness and rounded shape, derived from weathering during water transport. It has many advantages. For example, its particle sizes vary from 0.6 to 4.75 mm, and they have low percentages of dust, clay and other impurities, typically not more than 0.03%. The sand used in this experiment has a density of 1.6 g/cm^3 and a fineness modulus of 2.6. Figure 1 indicate the peaks of the specific element and their concentration in the river sand.

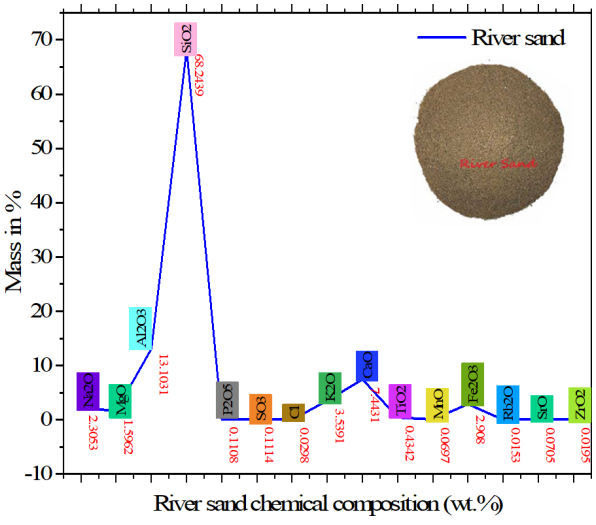

Fig. 1. Chemical composition of the river sand

(b) Artificial sand

Artificial sand (Figure 2) supplied by Gongyi Yuanhengjing Water Supply Factory in China was obtained by mechanically crushing natural stone. It consists of loose grains with no cohesion. The grain

Table 1. Fine aggregate gradation

Sieve size (mm) Gradation	%passing	Heat conductivity W/(m·C)	Purchase price in the Chinese market US$/kg	
0–0.6	20			
0.6–1.18	45	0.27	39	River sand
1.18–2.36	25	0.05	49	Artificial sand
2.36–4.75	10	0.12	90	Basalt sand

Table 2. CSA chemical composition weight in percentage

CaO	Al_2O_3	SO_3	SiO_2	Fe_2O_3	MgO	TiO_2	K_2O	SrO	Na_2O	Cl	P_2O_5
519.4	86.2	86.2	40.5	80.0	13.1	5.1	6.8	59.9	0.5	1.3	0.5
45.28%	17.51%	15.76%	9.19%	2.50%	1.90%	0.75%	0.48%	0.17%	0.19%	0.11%	0.10%

Table 3. Mixing of the mortar samples

Number of samples	CSA (g)	water	Different type of sand (g) River, Basalt, Artificial	water/cement ratio	Temperature °C
36 (12 for each type of sand)	450	225	1350	0.5	20,100,200,300

sizes vary from 0.15 to 4.7 mm, and, like natural sand, artificial sand can be fine.

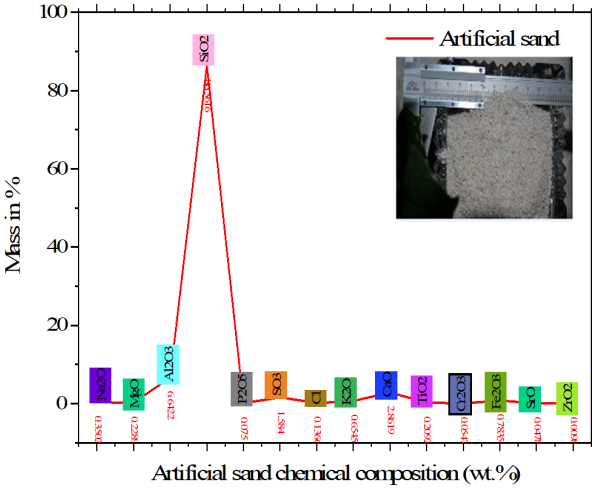

Fig. 2. Chemical composition of the artificial sand

(c) Basalt sand

Figure 3 shows the basalt rock used in this study, which also came from Gongyi Yuanhengjing Water Supply Factory in China. The SiO_2 content varies between 45% and 52%, and the $K_2O + Na_2O$ content is more combined with rock, CaO, and $Fe_2O_3 + FeO$. As a building material, basalt has excellent strength and stability, good wear resistance, and low water absorption [32]. It is also a very good architectural material; it is widely used for indoor and outdoor decoration, mainly as outdoor stone, as its color matches various other colors in decorations [33].

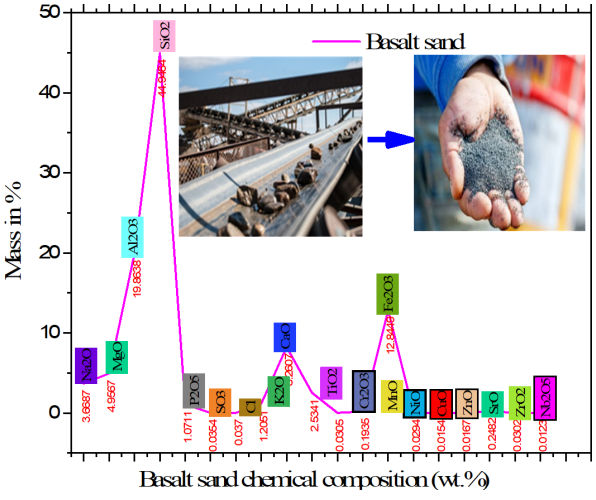

Fig. 3. Chemical composition of the basalt sand

The characteristics of the different fine aggregate gradations used in this study, with their price

in the Chinese market and their heat conductivity values, are shown in Table 1.

2.1.2. Calcium sulphoaluminate cement

CSA cement-42.5 with a specific surface area of 363 m^2/kg was used for all the preparations; its mineralogy is shown in Table 2. It is a cement with compressive strength and flexural strength at 28 days equal to 72.1 MPa and 50.2 MPa, respectively, with the initial setting time between 30~50 mins and final setting time 40~90 mins.

2.1.3. Mix proportions

The different mixes' design proportions are shown in Table 3.

2.2. Test method

Consistent with Chinese GB/T500081–2002 standard [34] test methods, which are the equivalent of BS EN 1015–methods of testing for mortar for masonry (a multi-part standard) and BS 4551–methods of Proper Masonry Field Testing ASTM C270 vs. C780, samples were cast and then demolded after 24 hours. For each group (RSM, ASM and BSM), we cast three 60×60×160 mm mortars. Three types of sand times three samples times four temperatures (20, 100, 200 and 300 degrees) makes 36 testing samples. After standard curing of 28 days, specimens were oven-dried until the mass change in half a day was 1 g. Then, the samples were exposed to elevated temperature at the rate of 4°C/min until they reached the target temperature. After that, the temperature was maintained for 4 hrs, then cooled down at the rate of 2°C/min inside the electronic furnace; then we performed the flexural and compressive strength calculations for the molded test samples.

3. Engineering properties

3.1. Compressive and flexural strength

The flexural (60×60×160 mm samples) and compressive strength of each group (RSM, ASM and BSM) were as measured, following the Chinese standard GB/T50080–2016 [35] which is equivalent to the standard-compliant flexural strength tests on mortar prisms, in accordance with EN 196 and ISO 679. The test was performed using a force-controlled testing machine to ensure an application of 50N/s +/−10N/s and 2400 N/s +/−200N up to rupture for the flexural and compressive strength, respectively.

3.2. Hydration mechanism observation

3.2.1. X-ray diffraction (XRD) analysis

Following the Chinese standard [36], we ran XRD testing. A Bruker D8A25 X-ray diffractometer was used to observe the phase change of the samples. The instrument uses 40kV and 40mA CuKα radiation. The scanning step length is 0.12°, the time of each step is 1s, and the diffraction angle range is 5–70°. We tested three samples of each group after exposure to different temperatures and reported the average value in this work. The results of XRD testing of each group, all gathered from the interior of each specimen, are presented in this study. They can help us understand better the strength decrease of the different mortars as the temperature rises, caused by the dehydration of the CSA cement.

3.2.2. SEM observations

The microstructure of the sample was observed by the Quanta FEG 250 scanning electron microscope after drying in a vacuum oven.

The microstructure of the mortars after exposure to different temperatures and after the completion of destructive testing was analyzed using SEM, which helps us visualize the microstructure of the dehydrated calcium sulfoaluminate mortar (CSAM) as the temperature increases. We tested three samples for each group after exposure to different temperatures. This enables us to describe the mechanical properties of the group of specimens correlated with the microstructure of the different mortars, to explore the influence of different fine aggregate usage schemes on the anti-cracking performance of CSA concrete.

3.2.3. Element ratios from EDS analyses

In the EDS line scan analysis following a Chinese standard [37], the electron beam scans the sample along a line to obtain it depicts or visual-

Table 4. Strength of the different samples

Strength (MPa)		Heating temperature/°C					
		Reference sample	Standard deviation of the compressive strength and flexural strength at 20°C	100°C	Standard deviation of the compressive strength and flexural strength at 100°C	Loss rate %	
RSM NAC	Compressive strength	21	1.55	10.8	1.17	48.6	
	Flexural strength	4.7	1.00	3.7	1.36	21.3	
ASM NAC	Compressive strength	25	3.43	22.1	1.02	11.6	
	Flexural strength	5.9	0.78	5.4	0.68	8.5	
BSM NAC	Compressive strength	27.1	3.88	14.8	0.82	45.4	
	Flexural strength	5.1	0.97	4.9	0.85	3.9	
Strength (MPa)		Heating temperature/°C					
		200°C	Standard deviation of the compressive strength and flexural strength at 200°C	Loss rate %	300°C	Standard deviation of the compressive strength and flexural strength at 300°C	Loss rate %
RSM NAC	Compressive strength	6.3	0.40	70	5.2	0.76	75.2
	Flexural strength	1.2	1.46	74.5	1.2	0.42	74.5
ASM NAC	Compressive strength	6.9	0.98	72.4	5	1.75	80
	Flexural strength	1.5	0.05	74.6	0.8	0.41	86.4
BSM NAC	Compressive strength	5.66	1.29	79.1	3.05	1.21	88.7
	Flexural strength	2	0.34	60.8	1.8	0.33	64.7

izes the change in elements. Combined with sample morphology and control analysis, it can visually obtain the distribution of elements in different regions. We tested three samples of each group after exposure to different temperature. We arbitrarily selected two specific points on the different mortar sample to evaluate the atomic ratios inside the different samples as the temperature increased.

3.2.4. TG testing

To understand the recorded strength in terms of chemical decomposition of the CSA cement provoked by thermal treatment, TG was performed. We tested three samples of each group after exposure to different temperatures. TG analysis following a Chinese standard was carried out in a Mettler Toledo apparatus operating in the temperature range of 30° to 800°C, with a heating rate of 10°C/min. Weight loss and heating rate were continuously recorded.

4. Results

4.1. Compressive and flexural strength

It can be seen from Table 4 that the compressive strength at room temperature of BSM mortar was slightly higher than that of ASM, while the compressive strength value of RSM was the lowest.

Table 5. Strength loss vs. temperature

	20°C	100°C		200°C		300°C	
		Strength MPa	Loss in %	Strength MPa	Loss in %	Strength MPa	Loss in %
RSM Compressive strength	21	10.8	(−)48.6	6.3	(−)70	5.2	(−)75.2
RSM Flexural strength	4.7	3.7	(−)21.3	1.2	(−)74.5	1.2	(−)74.5
ASM Compressive strength	25	22.1	(−)11.6	6.9	(−)72.4	5	(−)80
ASM Flexural strength	5.9	5.4	(−)8.5	1.5	(−)74.6	0.8	(−)86.4
BSM Compressive strength	27.1	14.8	(−)45.4	5.66	(−)79.1	3.05	(−)88.7
BSM Flexural strength	5.1	4.9	(−)3.9	2	(−)60.8	1.8	(−)64.7

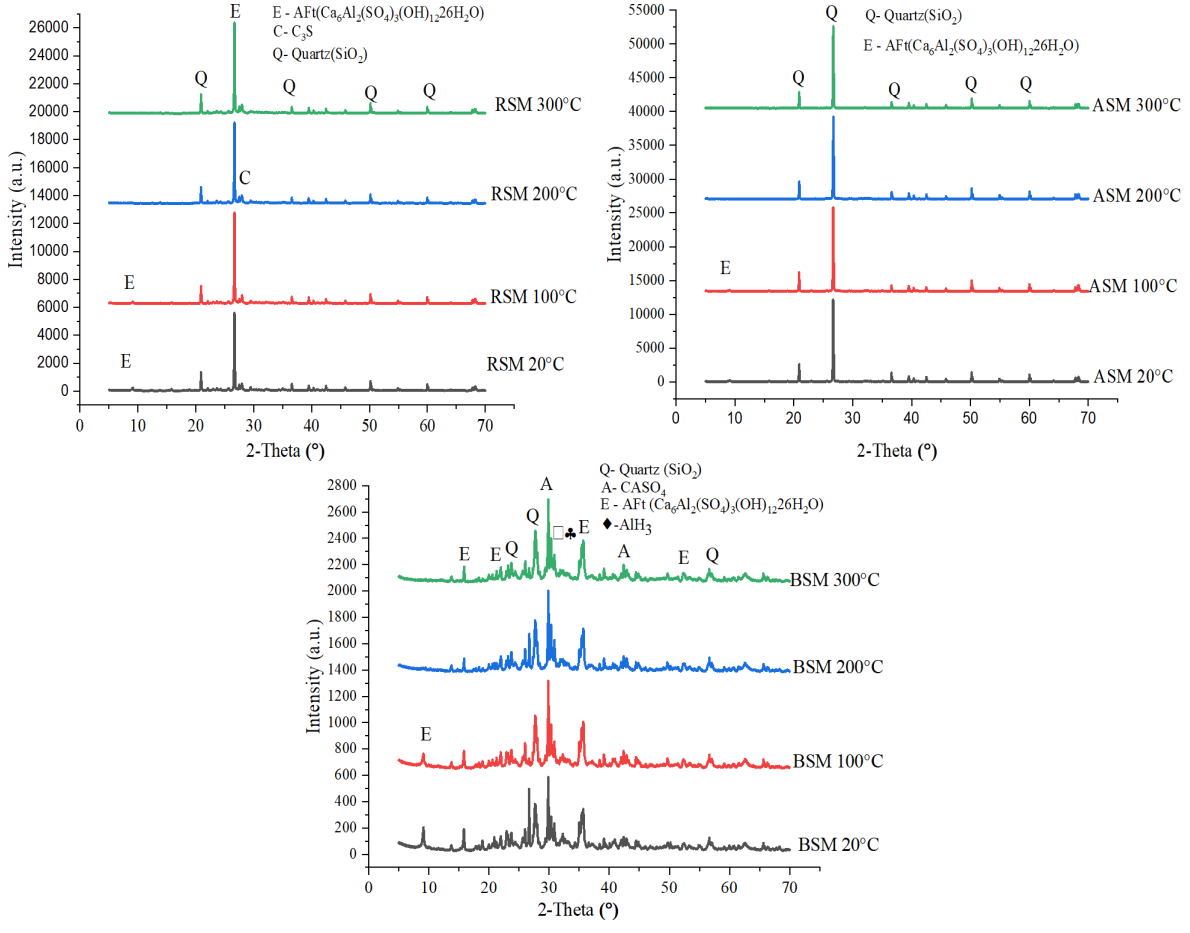

Fig. 4. XRD spectra

With the Standard deviation =

$$\sqrt{\frac{\sum_{i=0}^{n} f^2 ch,i \; - \; nm^2 fcu}{n-1}}$$

In the formula:

$f_{ch,i}$ stands for the strength value of the *i*th group of mortar specimens in the statistical period, MPa;

n stands for the number of groups of mortar specimens with the same strength standard value in the statistical period;

m_{fcu} stands for the average strength of n groups of mortar specimens in the statistical period, MPa.

The evolution of the three group mortars after high temperature treatment is shown in Table 5.

The loss value in terms of percentage was obtained by this formula: loss value = (initial strength – residual strength after high temperature heating) / initial strength. The compressive and flexural strength results show that the strength of mortars made from different sand types decreased by varying amounts at different exposure temperatures. The strength decreased moderately at 100°C, while at 200°C and 300°C, the strength dropped sharply.

4.2. X-ray diffraction (XRD) analysis

The XRD spectrums of Figure 4 indicate the chemical decomposition of the different mortars exposed to increasing temperatures. Pairs of new peaks appeared as the temperature increased, indicating ongoing chemical decomposition as the temperature rose. Narrow and sharp diffraction peak shapes were found in all the samples, at the temperature less 100°C. At the diffraction angles of 10°, the ettringite (AFt) crystal dehydrated at 100°C sample is more than the AFt crystal dehydrated in other samples. We have normalized our figures to the largest peak in each spectrum; the appearance or disappearance of peaks indicates either a change in the major peak or a change in the minor peak. The change reflects gain or loss associated with the crystalline compound.

The XRD results for the mortars were dominated by phase v = calcium aluminosilicate hydrate (C-A-S-H) gel ($CaAl_2Si_2O8.4H_2O$), n = quartz (SiO_2), l = calcite (CaCO3), and u = portlandite (Ca(OH)2). The highest peak in the CASH phase is at $2\theta = 26.6543°$, quartz at $2\theta = 20.8682°$, portlandite at $2\theta = 18.0569°$, and calcite at $2\theta = 29.4149°$ for the basalt. The basalt's highest peak in the CASH phase is found at $2\theta = 26.6568°$, quartz at $2\theta = 20.8737°$, portlandite at $2\theta = 18.8767°$, and calcite at $2\theta = 29.4174°$.

The main mineral components of the products of hydration were AFt and $CaSO_4$ and to a lesser degree, $CaCO_3$. However, after 100°C, the XRD spectrum changed significantly: the spike of the diffraction peaks of AFt at 2-Theta=9° (E) was the only AFt peak that disappeared. This was indicated in the ASM set, but not for RSM and BSM. The number of CaSO4 diffraction peaks decreased significantly, the intensity decreased, and the diffraction peak of CaCO3 appeared. This indicates that after 100°C, the mineral components of the CSA cement have obviously changed; the AFt has completely decomposed.

4.3. SEM crack observations

From Figure 5, it can be understood that under the action of heat, the micro-cracks constantly increased as the thermal stress gradually increased. When the temperature was less than 100°C, the number and size of the cracks were small; however, as the temperature increased, the number of cracks in the observed area of the test specimen increased, changing from fine cracks to macro-crack size. In addition, the number of fractures is important in the RSM samples.

The higher the heating temperature, the more cracking was observed, particularly inside the RSM. As the temperature rose, rapid crack expansion indicated an increase in sample brittleness, correlated with strength reduction. For the 200°C and 300°C test samples (RSM, ASM, and BSM) most of the cracks appeared as vertical; at 300°C, inside the test samples (RSM, ASM, and BSM) we could observe two-sided and larger intermediate oblique cracks.

As the temperature increased, free water and combined water gradually escaped, and the strength of the sample was reduced. When the temperature reached 200°C, the sample began to crack and some new pores formed. The main reason is that in a high-temperature state, water evaporation and hydrated product decomposition cause the capillary pore pressure to increase, thereby generating new cracks and propagating existing microcracks. As the temperature increased, cracks at the fine aggregate and CSA cement interface appeared more frequently. When the crack was extended to the CSA cement paste contact surface, the cracks tended to propagate along the whole capillary. After exposure to 300°C, the cracks were obvious. However, the crack density of RSM was much larger than that of ASM and BSM.

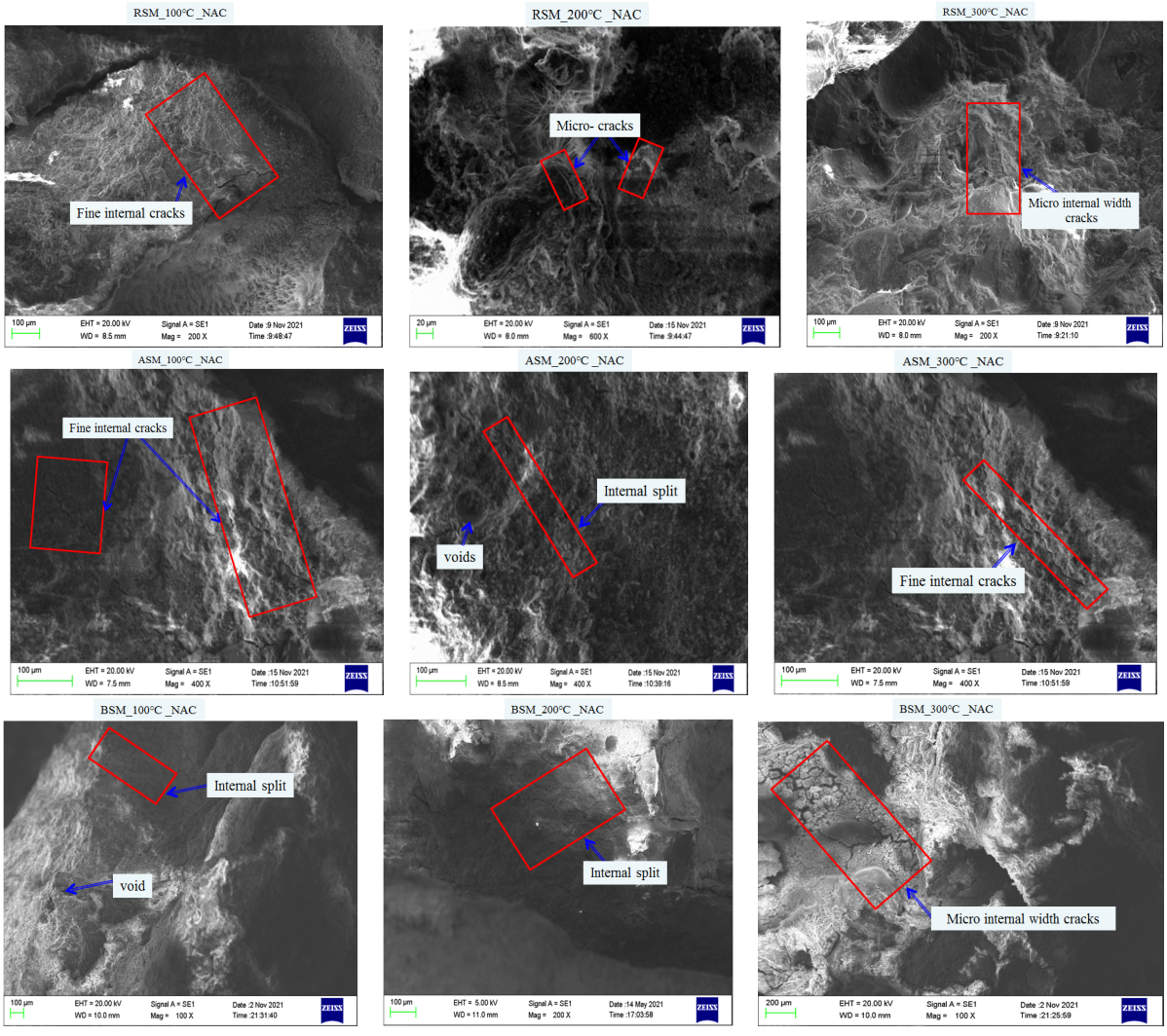

Fig. 5. Microscopic image of mortar sample after different temperature exposure

4.4. Experimental EDS ratios

Figure 6 shows the atomic constituency (typically O, Mg, AL, Si, S, K, Ca, Mg, and Fe) of the various mortars exposed to various temperatures. In most cases, the most prevalent element by mass was O. Different peaks were observed as the temperature rose. The strongest and weakest peaks of O, S, Si, and Al were observed in the 100°C specimens. This is caused by the presence of AFt, which decomposes. At room temperature for the entire group of samples, the Ca/Si ratio was higher than the ratio at 100°C. With the increase in conditioning temperature, the ratio of Ca/Si was found to change for RSM, ASM and BSM. Al was found in the spectrum of the different elements as the temperature rose.

Table 6 presents the element ratios for the EDS analyses of the different mortar samples. The results indicate that the samples contained the trace element of barium. Ye'elimite contains mainly barium and iron. The barium element can be also observed in belite solid solution, whereas it is not substituted in alite. To better understand the results, Table 6 elaborates the atomic ratios obtained by EDS. The result is in accordance with the XRD analysis presented earlier. The average atomic ratios (Ca/Si, Ca/Al and Ca/s) for the ASM and BSM increased with rising temperatures.

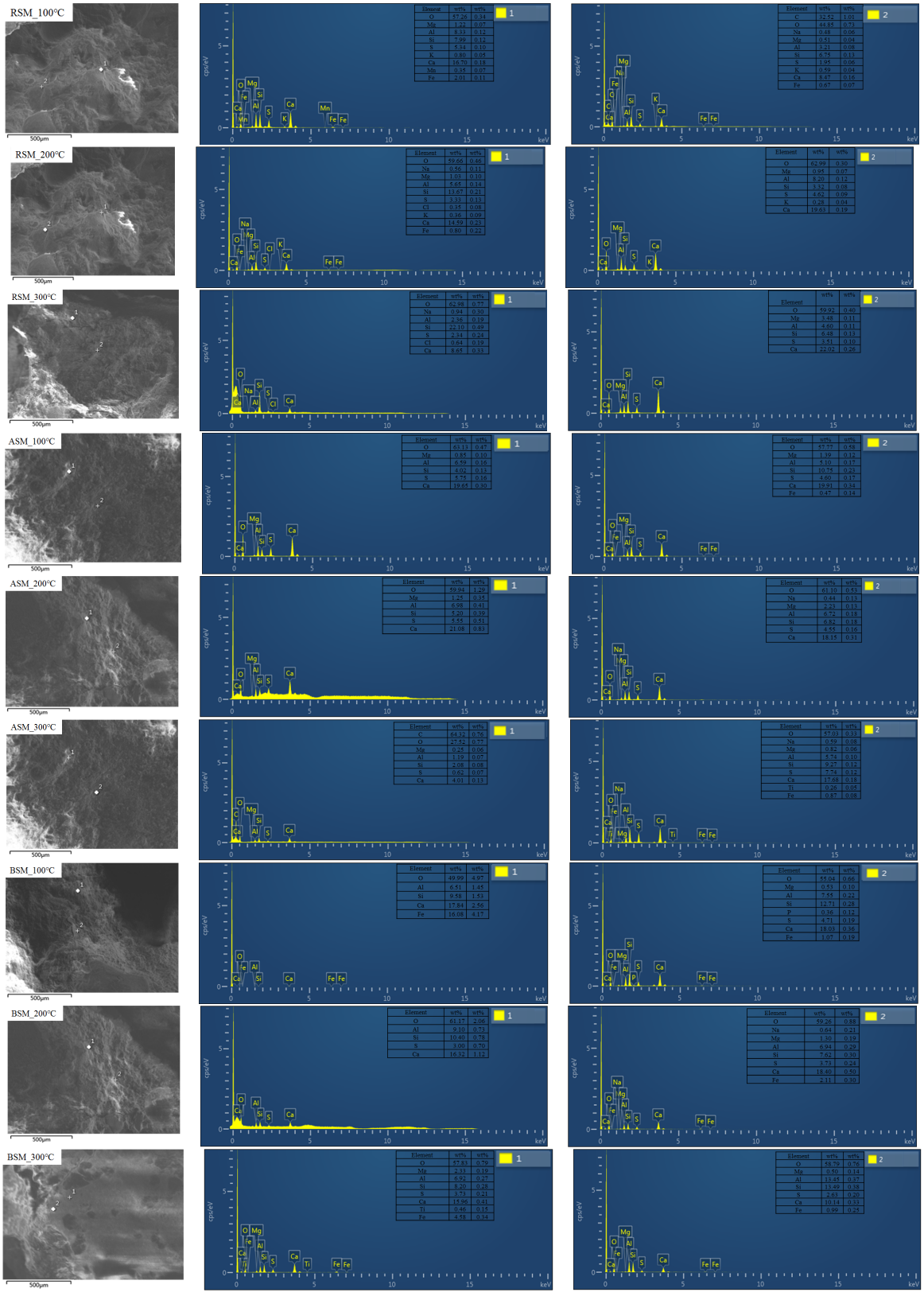

Fig. 6. EDS of the different CSA mortars when heated

Table 6. The average atomic ratios obtained by EDS in the different heated mortar samples

Experimental EDS ratios	Different sample	Ca/Si	Ca/Al	Ca/S
Belite Ye'elimite Alite	NAC_ RSM_ 100°C	3.04	6.75	7.36
Belite Ye'elimite Alite	NAC_ RSM_ 200°C	5.34	5.40	5.39
Belite Ye'elimite Alite	NAC_ RSM_ 300°C	0.36	0.68	3.64
Belite Ye'elimite Alite	NAC_ ASM_ 100°C	5.79	3.80	3.08
Belite Ye'elimite Alite	NAC_ ASM_ 200°C	3.92	2.83	6.85
Belite Ye'elimite Alite	NAC_ ASM_ 300°C	10.50	17.93	16.70
Belite Ye'elimite Alite	NAC_ BSM_ 100°C	5.16	7.41	8.40
Belite Ye'elimite Alite	NAC_ BSM_ 200°C	3.17	4.64	4.40
Belite Ye'elimite Alite	NAC_ BSM_ 300°C	130.35	33.76	12.91

Belite – C2S, Ye'elimite – $Ca_4Al_6O_{12}(SO_4)$, Alite – C3S, NAC – natural air cooling

4.5. Thermal analysis (TG testing)

Figure 5 shows that when the hydrated product was heated to 300°C, the decomposition formed more CH. Large endothermic valleys remained around 200°C due to the dehydration of the aluminum hydroxide (AH_3), and after that the rate of weight loss decreased. AFt and $Al(OH)_3$ disappeared at a slightly lower rate at 200°C and around 300°C, respectively. That amount decreased to 39% at 100°C and then completely disappeared beyond that point. Similarly, $Al(OH)_3$ represented 26% of the mass at 20°, 100°, and 200°C but disappeared at 300°C; this result is correlated with the lower strength measurements and lower mass weight loss between 100° and 300°C.

5. Discussion and significance

The reduction of compressive strength can be attributed to the separation of free water caused by high temperature and the decomposition of hydrophilic products. This result correlates with the research study published by Kouadjo where he observed a chemical decomposition of the CSA as temperature rises [38]. The difference in mechanical properties of mortars made from different sands can be attributed to the differences between the shape, particle size, and surface area of the sand. It was shown by Linzhu that the size and shape of the sand have a great influence on the mechanical properties of the material [39] as well as in the adhesion strength [40]. In fact, artificial sand and basalt rock sand both bind to the CSA cement better

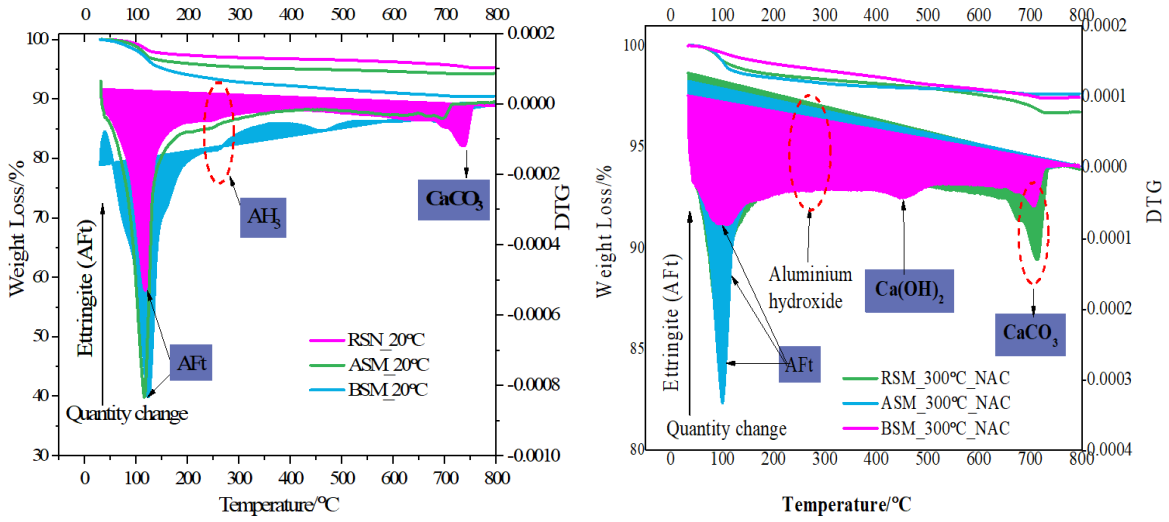

Fig. 7. TG of the different mortars

than river sand, as supported by the average results recorded in this work. Therefore, the use of artificial and basalt sand can improve the strength of CSA cement at reasonable cost, since the price of artificial sand is US $1.01 per kg, or only $0.74 per kg more than the cost of river sand. Under exposure to higher temperatures, the mechanical properties of ASM and BSM do not deteriorate as quickly as those of RSM. It can be seen from Table 4 and 5 that according to the comparison results of RSM, ASM, and BSM, as the temperature increases from 100° to 300°C, the crack resistance of the mortars drops greatly, as more cracks were found on the surface of the sample; the reason for this result is not only the grain shape of the machine-made sand itself but also its size [41]. The water evaporation of the surface mortar cannot be replenished in time, and it is easy to cause cracking [42]; as the cracks on the mortar surface are narrow [43]. Based on microscopic observations, the crack resistance of the ASM and BSM is higher than that of RSM. The reason for this result is the grain shape of the artificial sand. The RSM on the sample surface had issues with evaporating moisture in time, which easily causes the appearance of more cracks in comparison to the ASM and BSM. We observed that the ASM and BSM specimens' crack resistance was higher than the RSM, and the total crack length per unit area of the two specimens was similar. For the RSM, the specimen surface cracks are wider (the maximum crack width is 0.4mm) and the characteristic length is shorter, whereas for the ASM specimens, the surface cracks are narrow (the maximum crack width is 0.2mm) and the length is longer.

6. Conclusion

In this experiment, river, artificial, and basalt sand were used as the fine aggregate in mortar. The three different types of fine aggregates were subjected to descriptive tests of the strength, crack resistance diffraction (XRD) analysis, and TG. We sought to characterize the impact of different fine aggregate use schemes on the mechanical properties and durability of RSM, ASM, and BSM when heated.

1. The compressive strength of BSM mortar was slightly higher than that of ASM, while the compressive strength value of RSM was the lowest. The evolution of the three group mortars after exposure to high temperature shows that the compressive strength of different sand types decreased in varying degrees at different exposure temperatures. The compressive strength decreased slowly at 100°C, while at 200°C and 300°C, it dropped sharply.

2. Under the action of heat, micro-cracks occurred constantly, increasing in number as the thermal stress gradually increased. When the temperature was below 100°C, the number and size of cracks in the test sample were small; however, as the temperature increased, the number of cracks in the observed area of the test specimen increased and the cracks also changed from micro to macro in size.
3. At room temperature for the entire sample group, the Ca/Si ratio was higher than the other ratios at 100°C. The average atomic ratios (Ca/Si, Ca/Al and Ca/s) for the ASM and BSM increased with rising temperature. The decomposition of hydrated product at 300°C formed more calcium hydroxide (CH). Large endothermic valleys remained around 200°C due to the dehydration of the aluminum hydroxide (AH_3), and after that the rate of weight loss decreased. AFt and $Al(OH)_3$ disappeared at a little less than at 200°C and around 300°C, respectively, for the different specimens.

Acknowledgements

The authors gratefully acknowledge the financial support from the Shandong Provincial Higher Education Youth Innovation Team Program of China (2022KJ284), and the supported of Taishan Scholars Program of China.

References

[1] Wiggenhauser H, Köpp C, Timofeev J, Azari H. Controlled Creating of Cracks in Concrete for Nondestructive testing. *Journal of Nondestructive Evaluation.* 2018; 37: 67. https://doi.org/10.1007/s10921-018-0517-x

[2] Huynh T P, Vo D H, Hwang C L. Engineering and durability properties of eco-friendly mortar using cement-free SRF binder. *Construction and Building Materials.* 2018; 160:145-155. https://doi.org/10.1016/j.conbuildmat.2017.11.040

[3] Hasar U C, Izginli M, Ozturk H, Korkmaz H, Cevik A, Irshidat M R. Surface curing effect on reflection response of hardened cementitious mortar samples. *Measurement.* 2021; 185: 110026. https://doi.org/10.1016/j.measurement.2021.110026

[4] Hossain M M, Karim M R, Hossain M K, Islam M N, Zaina M F M. Durability of mortar and concrete containing alkali-activated binder with pozzolans: A review. *Construction and Building Materials.* 2015; 93: 95-109. https://doi.org/10.1016/j.conbuildmat.2015.05.094

[5] Lee H S, Balasubramanian B, Gopalakrishna G V T, Kwond S J, Karthick S P, Saraswathy V. Durability performance of CNT and nanosilica admixed cement mortar. *Construction and Building Materials.* 2018; 159: 463-472. https://doi.org/10.1016/j.conbuildmat.2017.11.003

[6] Soulios V, Jan de Place Hansen E, Peuhkuri R, Møller E, Ghanbari-Siahkalic A. Durability of the hydrophobic treatment on brick and mortar. *Building and Environment.* 2021; 201: 107994. https://doi.org/10.1016/j.buildenv.2021.107994

[7] Baali L, Naceri A, Rahmouni Z, Mehidi M W N. Experimental Study of the Possibility to Make a Mortar with Ternary Sand Natural and Artificial Fine Aggregates. *International Conference on Physics Science and Technology.* 2011; 1875-3892 doi:10.1016/j.phpro.2011.11.044

[8] Abdelrahman, Abushana, Alnahhal W. Combined effects of treated domestic wastewater, fly ash, and calcium nitrite toward concrete sustainability. *Journal of Building Engineering.* 2021; 44: 103240. https://doi.org/10.1016/j.jobe.2021.103240

[9] Kim Y Y, Lee K M, Bang J W, Kwon S J. Effect of W/C Ratio on Durability and Porosity in Cement Mortar with Constant Cement Amount. *Advanced material science engineering.* 2014; 273460. https://doi.org/10.1155/2014/273460

[10] Antoni A, Chandra L, Hardjito D. The Impact of Using Fly Ash, Silica Fume and Calcium Carbonate on the Workability and Compressive Strength of Mortar. *Procedia Engineering.* 2015; 125:773-779. https://doi:10.1016/j.proeng.2015.11.132

[11] Kwon S J, Feng M Q, Park S S. Characterization of electromagnetic properties for durability performance and saturation in hardened cement mortar. *NDT&E International.* 2010; 86–95. https://doi.org/10.1016/j.ndteint.2009.09.002

[12] Maria da Luz Garcia, Sousa-Coutinho J. Strength and durability of cement with forest waste bottom ash. *Construction and Building Materials*. 2013; 41: 897–910. https://doi.org/10.1016/j.conbuildmat.2012.11.081

[13] Bogas A J, Gomes A. A simple mix design method for structural lightweight aggregate concrete. *Materials and Structures.* 2013; 46: 1919–1932. https://doi.org/10.1617/s11527-013-0029-1

[14] Fahmi H M, Polivka M, Bresler B. Effects of sustained and cyclic elevated temperature on creep of concrete. *Cement and Concrete Research.* 1972, 2(5): 591-606. https://doi.org/10.1016/0008-8846(72)90113-5

[15] Cagnon H, Vidal T, Sellier A. Transient thermal deformation of high performance concrete in the range 20°C–40°C. *Cement and Concrete Research*. 2019, 116: 19-26. https://doi.org/10.1016/j.cemconres.2018.11.001

[16] Liu S, Kong Y, Wan T. Effects of thermal-cooling cycling curing on the mechanical properties of EVA-modified concrete. *Construction and Building Materials*. 2018, 165: 443-450. https://doi.org/10.1016/j.conbuildmat.2018.01.060

[17] Oje A M, Ogwu A A, Rahman S U. Effect of temperature variation on the corrosion behavior and semiconducting properties of the passive film formed on chromium oxide coatings exposed to saline solution. *Corrosion Science*. 2019, 154: 28-35. https://doi.org/10.1016/j.corsci.2019.04.004

[18] Díaz B, Guitian B, Novoa X R. The effect of long-term atmospheric aging and temperature on the electrochemical behavior of steel rebar's in mortar. *Corrosion Science*. 2018, 140: 143-150. https://doi:10.1016/j.corsci.2018.06.007

[19] Zhu N, Jin F, Kong X, Xu Y, Zhou J, Wang B, Wu H. Interface and anti-corrosion properties of sea-sand concrete with fumed silica. *Construction and Building Materials.* 2018, 1085-1091. https://doi.org/10.1016/j.conbuildmat.2018.08.040

[20] Yu H; Meng T, Zhao Y, Liao J, Ying K. Effects of basalt fiber powder on mechanical properties and microstructure of concrete. *Case Studies in Construction Materials.* 2022, e01286. https://doi.org/10.1016/j.cscm.2022.e01286

[21] Zhang J, Li D, Wang Y. Toward intelligent construction: Prediction of mechanical properties of manufactured-sand concrete using tree-based models. *Journal of Cleaner Production.* 2020, 120665. https://doi.org/10.1016/j.jclepro.2020.120665

[22] Dobiszewska M, Robert W. Barnes. Properties of Mortar Made with Basalt Powder as Sand Replacement. *Materials Journal.* 2020, 3-9.

[23] Tchekwagep J J K, Shoude W, Mukhopadhyay A K, Shifeng H, Xin C .The Impact of Extended Heat Exposure on Rapid Sulphoaluminate Cement Concrete Up To 120°C. *Periodica Polytechnica Civil Engineering.* 2021;18. https://doi.org/10.3311/PPci.17122

[24] Tchekwagep J J K, Piqi Z, Shoude W, Shifeng H, Xin C. The impact of changes in pore structure on the compressive strength of sulphoaluminate cement concrete at high temperature. *Materials Science Poland.* 2021; 75 – 85. https://doi:10.2478/msp-2021-0006

[25] Tchekwagep J J K, Shoude W, Mukhopadhyay A K, Shifeng H, Xin C.2020. Strengths of Sulphoaluminate Cement Concrete and Ordinary Portland cement Concrete after Exposure to High Temperatures. *Ceramics-Silikáty.* 2020; 227-238. https://doidoi:10.13168/cs.2020.0012

[26] Tchekwagep J J K, Shoude W, Mukhopadhyay A K, Huang S, Xin C. Compressive strength of rapid sulphoaluminate cement concrete exposed to elevated temperatures. *Ceramics-Silikáty.* 2020; 299-309. https://doi.org/10.13168/cs.2020.0019

[27] Swaidani A M; Baddoura M K; Aliyan S D; Choe W. Assessment of Alkali Resistance of Basalt Used as Concrete Aggregates. *Journal of civil engineering.* 2015, 10, https://doi:10.1515/sspjce-2015-0014

[28] Akhtar M N, Ibrahim Z, Muhamad B Ni, Jameel M, Tarannum N, Akhtar J N. Performance of sustainable sand concrete at ambient and elevated temperature. *Construction and Building Materials.* 2021, 122404. https://doi.org/10.1016/j.conbuildmat.2021.122404

[29] Yi H, Oh K, Kou R, Qiao Y. Sand-filler structural material with a low content of polyethylene binder. *Sustainable Materials and Technologies.* 2020, e00194. https://doi.org/10.1016/j.susmat.2020.e00194

[30] Cabrera O H D , FIrassar E. High-strength concrete with different fine aggregate. *Cement and Concrete Research.* 2002, 1755-1761. https://doi.org/10.1016/S0008-8846(02)00860-8

[31] Singh S, Nagar R, Agrawal V. A review on Properties of Sustainable Concrete using granite dust as replacement for river sand. *Journal of Cleaner Production*. 2016, 74-87. https://doi.org/10.1016/j.jclepro.2016.03.114

[32] Branston J, Das S, Kenno S Y, Taylor C. Mechanical behavior of basalt fiber reinforced concrete. Construction and Building Materials, 2016, 878-886. https://doi.org/10.1016/j.conbuildmat.2016.08.009

[33] Rostásy F S, WeiβG R, Wiedemann. Changes of pore structure of cement mortars due to temperature. *Cement and Concrete Research*. 1980, 10: 157-164. https://doi.org/10.1016/0008-8846(80)90072-1

[34] Jiansheng S, Xi G, Bo L, Kun D, Ruoyu J, Wei C, Yidong X. Damage Evolution of RC Beams Under Simultaneous Reinforcement Corrosion and Sustained Load. *Materials (Basel)*. 2019, 12(14):627. doi: 10.3390/ma12040627

[35] Yufeng F, Qiang Z, Dengquan W. Comparing Permeability and Drying Shrinkage of the Concrete Containing Mineral Admixtures under the Equal Strength Grade. *Minerals*. 2022, 12(11), 1477; https://doi.org/10.3390/min12111477

[36] Jolanta B L, Piotr B, Jarosław B, Roman B, Elżbieta H. Effects of Elevated Temperatures on the Properties of Cement Mortars with the Iron Oxides Concentrate. *Materials* (Basel). 2021 Jan; 14(1): 148. https://doi:10.3390/ma14010148

[37] Deqiang Y, Changwang Y, Shuguang L, Zhirong J, Chunguang W. Prediction of Concrete Compressive Strength in Saline Soil Environments. *Materials (Basel)*. 2022; 15(13): 4663. doi: 10.3390/ma15134663

[38] Kouadjo Tchekwagep J J, Dangui C, Mukhopadhyay A K, Shoude W, Shifeng H, Xin C. Quantitative Rietveld analysis of the decomposition of hardened rapid sulphoaluminate cement after exposure to elevated temperatures. *Archives of Civil and Mechanical Engineering*. 2021, 119. https://doi.org/10.1007/s43452-021-00265-9

[39] Linzhu L, Magued I. Evaluation of Roundness Parameters in Use for Sand. J. Geotech. *Geoenviron. Eng*.

2021, 147(9). https://doi.org/10.1061/(ASCE)GT.1943-5606.0002585

[40] Khan M, Abbas H. Performance of concrete subjected to elevated temperature. *European Journal of Environmental and Civil Engineering*. 2016, 20: 532-543. https://doi.org/10.1080/19648189.2015.1053152

[41] Maanser A, Benouis A, Ferhoune N. Effect of high temperature on strength and mass loss of admixtured concretes. *Construction and Building Materials*. 2018, 166:916-921. https://doi.org/10.1016/j.conbuildmat.2018.01.181

[42] Faisal A, Waleed A, Qais F. Effect of high temperature and type of cooling on some mechanical properties of cement mortar. MATEC Web of Conferences. 2018, 162. https://doi.org/10.1051/matecconf/201816202010

[43] Safaa A M, Rwayda K S A, Teba T K. Investigating the effect of elevated temperatures on the properties of mortar produced with volcanic ash. *Innovative Infrastructure Solutions*. 2020, 20, 1. https://doi.org/10.1007/s41062-020-0274-4

Received 2022-11-20
Accepted 2023-02-10